The structure and composition of the annular modes in an aquaplanet general circulation model

Benjamin A. Cash, Paul J. Kushner and Geoffrey K. Vallis

GFDL, Princeton University

Princeton, NJ, 08542

Submitted to J. Atmos. Sci.: November 16, 2001

Revised: August 30, 2002

Abstract

The annular mode simulated by an atmospheric general circulation model with a zonally symmetric lower boundary is investigated. The annular mode, defined as the leading EOF of the zonal-mean surface pressure, has a meridional structure consisting of a north-south dipole, similar to observations. The leading EOF of the zonally varying surface pressure has the same meridional structure and is also zonally symmetric. Because the lower boundary is zonally symmetric, composites of days with high projection onto the mode have, to within sampling error, no zonal structure. However, individual periods during which the zonal-mean surface pressure projects strongly onto the annular mode are dominated by zonally localized structures. Thus, the model annular mode represents a zonally homogeneous distribution of zonally localized events with a similar meridional structure, rather than a zonally symmetric mode of variability *per se*. Individual annular-mode events typically show a north-south teleconnection pattern whose meridional structure closely resembles the annular mode and whose zonal structure extends 60 to 90 degrees in longitude, with a slight northwest-southeast offset between its centers of action. Similar structures are found for EOFs calculated over a subset of the domain corresponding to the width of the Atlantic basin. The spatial structure of both the teleconnection pattern and the regional EOFs resemble the observed North Atlantic Oscillation pattern.

1 Introduction

A long-standing goal of atmospheric research is to understand the dynamics of extratropical low-frequency variability. This type of variability is characterized by time scales of 10 days or greater, and by a relatively small number of 'teleconnection' patterns that seem to account for much of the variability (Barnston and Livezey, 1987). Teleconnections are generally defined as widely separated regions of high simultaneous correlation (e.g., Wallace and Gutzler, 1981). One of the most prominent Northern-Hemisphere teleconnections is the North-Atlantic Oscillation, or NAO (e.g., van Loon and Rogers, 1978; Wallace and Gutzler, 1981; Barnston and Livezey, 1987). The NAO pattern at the surface consists of a dipole in the pressure field, with a localized center near Iceland at 65°N and a broader region of opposite sign extending the width of the Atlantic near 40°N (Fig. 1). The NAO is the only teleconnection prominent throughout the entire year, and accounts for approximately 10% of the total NH low-frequency variability (Barnston and Livezey, 1987). The NAO influences temperature and precipitation over wide regions of Europe and North America (Hurrell, 1996; Hurrell and van Loon, 1997), making it of interest to researchers and forecasters alike.

In recent years, the nature of the NAO and its dynamics has been a subject of debate. A central concern is the apparent link between the NAO and the leading EOF of the Northern-Hemispheric extratropical surface pressure, which is known as the "Northern-Hemisphere annular mode", or NAM (Thompson and Wallace,

1998, 2000). The NAM has a strong, zonally symmetric center poleward of 65°N, weaker centers of opposite sign over the North Pacific and North Atlantic near 40°N, and an accompanying equivalent-barotropic vertical structure that extends into the stratosphere. Its structure in the North-Atlantic sector and its temporal variability are strongly correlated with those of the NAO. The NAM closely resembles its Southern-Hemisphere counterpart, the Southern-Hemisphere Annular Mode, or SAM (see Gong and Wang, 1999; Thompson and Wallace, 2000). The SAM is more zonally symmetric near the surface than the NAM, which is presumably due to the greater zonal asymmetry of the NH lower boundary. Both the SAM and the NAM become increasingly zonal with height.

The resemblance between the SAM and NAM suggests that they arise from similar dynamical processes governing atmospheric low-frequency variability and the maintenance of the zonal-mean extratropical circulation. There is a debate in the literature (e.g., Wallace, 2000; Ambaum et al., 2001) as to whether the SAM and NAM are fundamentally zonally symmetric or asymmetric modes of variability. From the former viewpoint, the NAO appears as a local manifestation of the global-scale annular-mode dynamics, rather than a locally determined dynamical pattern.

With the link between the NAO and the NAM as a central concern, we investigate here the structure of the annular-mode pattern and the composition of individual annular-mode 'events' simulated by an atmospheric general circulation model with a zonally symmetric lower boundary. Annular mode 'events' are here

defined as periods of several days with strong projections onto the annular mode; that is, periods when the principal component of the EOF defining the annular mode has a particularly high value (precise definitions are given in section 3). A model with zonally symmetric boundary conditions can be expected to be particularly amenable to the production of zonally symmetric modes of variability. Indeed, annular modes are credibly simulated in a number of comprehensive general circulation models and idealized atmospheric models (see Robinson, 1991b; Yu and Hartmann, 1993; Feldstein and Lee, 1996; Limpasuvan and Hartmann, 2000). One of our main aims is to describe the characteristic three-dimensional structure of the flow on days in which the annular mode is prominent, and in particular, in the longitudinal structure of these events. Our focus on individual annular-mode events and on this time scale is motivated in part by recent studies of the Pacific-North American teleconnection pattern and the NAO (Cash and Lee, 2001; Feldstein, 2000). These studies show that extratropical teleconnections evolve on timescales of 10 days to two weeks, and that analyzing them using monthly averages, as is quite commonly done, can produce a misleading picture of their dynamics.

We are also motivated by a concern that EOFs may give a misleading impression of the structure of the underlying data especially if the data is time averaged (the problem can be particularly pronounced in unrotated EOFs (see Richman, 1986), which are used to define the NAM and SAM). Our goal in this paper, then, is to see whether a model that is conducive to the production of zonally symmet-

ric modes of variability does in fact do so, and to further explore the structure of actual events that give rise to the annular mode of the model. The paper is organized as follows. Section 2 presents a description of the model and its simulated climate. Section 3 describes the structure of the annular mode. Section 4 analyzes the low-frequency variability using a one-point correlation map technique, and section 5 presents a summary and conclusions.

2 Model Description and Simulation Characteristics

We use an atmospheric general circulation model coupled to a globally uniform 40 m slab mixed-layer ocean model. This kind of model is sometimes referred to as an "aquaplanet" model. In this configuration, the ocean surface temperatures are predicted rather than prescribed, which we take to be important for a dynamically self-consistent representation of the climate system. The atmospheric model uses the spectral transforms method in the horizontal and the Simmons and Burridge (1981) finite-difference method in the vertical. The horizontal resolution is T42 (roughly 3° in latitude and longitude) and the vertical spacing consists of 14 sigma levels, with 5 levels corresponding to pressure levels higher than 300mb (i.e., roughly in the stratosphere). The model includes full radiative and moist-processes packages that similar to those used previously in GFDL climate models (e.g., Manabe et al., 1979). The model is forced by seasonally varying insolation. This leads, in the presence of the 40 m mixed layer, to a relatively weak seasonal

cycle. After four years of spin-up, radiative balance has been achieved and the seasonally varying ocean surface temperature has equilibrated. Subsequently, the model is run out for an additional 60 years. From the daily-sampled output from the model, we create a 10-day low-pass filtered time series, which is used as input to the EOF and other calculations. The seasonal cycle is removed from the time series by subtracting off the calendar mean at each day.

Examination of the model climatology shows that the model has effectively homogeneous statistics in the zonal direction, as expected under these boundary conditions. In addition, the Northern Hemisphere (NH) and Southern Hemisphere (SH) are statistically identical, modulo a half-year lag that is associated with the annual cycle of insolation. We create climatologies that pair NH January with SH July, NH February with SH August, and so on, effectively doubling, to 120, the number of samples of a given season. We parochially adopt the convention of defining the seasons in NH terms: that is, winter is December-January-February.

The climatological zonal-means of ocean-surface temperature, surface zonal wind, 200 mb zonal wind, and 200 mb meridional wind are shown as a function of calendar month in Fig. 2. Overall, the extratropical jets are somewhat stronger and shifted further equatorward than is observed. The pole-to-equator ocean surface-temperature difference has a weak maximum throughout winter and spring (Fig. 2a), and near-surface westerlies show a similar behavior (Fig. 2b). However, the upper-level winds (Fig. 2c) and Hadley cell (inferred from Fig. 2d)

are strongest in spring, and both near-surface and upper-level zonal winds are located furthest equatorward and closest to the Hadley cell in that season. Aspects of the model seasons are thus slightly out of phase with the observed, occurring slightly later with respect to the annual cycle of insolation. This can be attributed to the thermal inertia of the 40 m mixed-layer ocean, which weakens the seasonal cycle and introduces longer lags than in the real atmosphere.

The model's low-frequency variability also exhibits a seasonal variation, and now the model variability is more in phase with observations. For example, the variance of the de-seasonalized 10-day low-pass filtered surface pressure is stronger in winter (December–February) than spring (March–May) (see Fig. 3). Since our focus is on the annular modes as characteristic patterns of atmospheric low-frequency variability, we focus most of our analysis on the winter season, when this variability is strongest.

3 Annular Mode and Annular-Mode Events

3.1 Annular Mode

We define the annular mode as the leading EOF of the daily sampled, 10-day low-pass filtered, de-seasonalized, zonal-mean surface pressure for the winter hemisphere. The surface pressure covariance matrix includes area weighting by the cosine of latitude. We define an annular-mode "event" as 7 or more consecutive days in which the zonal-mean surface pressure projects onto the annular-

mode pattern with an amplitude greater than one standard deviation of the EOF's principal component time series. Events with positive projection are referred to as high-index events and events with negative projection are referred to as low-index events.

The annular-mode EOF is shown in Fig. 4a; it is normalized to have unit amplitude. The small amplitude of the mode at high latitudes is associated with the area weighting of the covariance matrix. To describe the typical relationship between the annular mode and the data, we regress the unweighted surface pressure field against the principal component time series. The regressed surface pressure response to one standard deviation of the principal component is shown in Fig. 4b. The simulated mode has maxima of opposite sign in the polar regions and midlatitudes, with the zero point falling near 50°. The overall structure is similar to the observed annular mode, but is shifted equatorward along with the mean circulation. This pattern accounts for a very large fraction, 76%, of the total variance of the zonal-mean low-pass filtered surface pressure. For comparison, a regression map of the surface pressure for the leading EOF of the zonally *varying* surface pressure is shown in Fig. 4c. Its meridional structure is essentially identical to that of Fig. 4b, and its lack of zonal structure reflects the zonal homogeneity of the sample. Departures from zonal symmetry decrease as the integration is lengthened. The EOF of the zonally varying surface pressure accounts for only 20% of the total variance. The sharp drop in explained variance between the leading EOFs of the zonal mean and zonally varying surface pressure indicates

that variations in the zonal mean surface pressure account for a relatively small fraction of the total variance of the surface pressure, a point consistent with the results below.

Composites, defined as the arithmetic mean taken over high-index events, produce a zonally symmetric structure similar to that of the annular mode (Fig. 5a); composites for low-index events produce the same pattern with a change of sign (Fig. 5b). This is expected from zonal homogeneity. Composites of other tropospheric variables, such as the zonal winds (Figs. 6a,b), reveal vertically coherent, equivalent-barotropic structures. In the wind field, the structure is that of a north-south dipole, similar to that obtained by regressing the zonal-mean wind on the annular-mode principal component time series. Comparing the total wind field (mean plus composite anomaly) for the high- and low-index states (Figs. 6c,d), we see that the axis of the westerly wind maximum is more strongly tilted upward and equatorward in the high-index state. This indicates that the baroclinic-eddy driven jet and the subtropical jet are more highly separated in latitude in the high-index state. The separation of the jets in the high-index state is still more pronounced in the observations (Ambaum et al., 2001), but the simulation captures the qualitative behavior.

3.2 Annular-Mode Events

Although the leading EOF of the zonally varying surface pressure (Fig. 4c) and the composites of the high- and low-index surface-pressure anomalies (Fig. 5)

are, to within sampling error, zonally symmetric, the question remains as to how representative these maps are of the structure of individual annular-mode events. When we examine the structure of individual high-index and low-index events, we see distinct, zonally localized structures (see Fig. 7 for examples). We find 71 high-index and 64 low-index events in the integration, all of which show strong deviations from zonal symmetry. As seen in the examples in Fig. 7, individual events typically have one to four centers at a given latitude, with the meridional locations of the maxima coinciding with those of the annular mode, and with opposite sign on either side of location of the node of the zonal-mean annular mode, which is at 50° latitude. More generally, we note the substantial distinction between the structure of the annular mode itself and the structure of the events that comprise it.

In order to quantify the degree of zonal asymmetry of individual annular-mode events, we compare, for individual events, the average amplitude of the zonal component of the flow to the average amplitude of the eddy component of the flow. To do so, we first remove all fourier components greater than zonal wavenumber four from the field. These smaller-scale components represent a noisy residual from the synoptic-scale variability that is largely truncated by the low-pass time filter — some of these weak small-scale features can be seen in Fig. 7. Averages are taken over the set of all high- and low-index events, and are compared to the full winter average (Figs. 8a–c). As expected from our definition of the annular mode, the high- and low-index averages show somewhat larger

amplitudes for the zonal-mean component of the flow than the full-winter average. The main point demonstrated in Fig. 8, however, is that eddies dominate the flow field over most of the extratropics, even on those days with high projections onto the annular mode. Models with zonally symmetric boundary conditions are known to support robust zonally asymmetric variability (Hendon and Hartmann, 1985; Robinson, 1991a). However, the dominance of the zonally asymmetric variability over the zonal mean in Figs. 7 and 8 indicates that the annular mode is an average over events of varying degrees of zonal localization.

4 Longitudinal structure of the simulated low-frequency variability

Given the mismatch between the zonal symmetry of the annular-mode pattern and the zonal asymmetry of the annular-mode events, we have explored alternative approaches to characterizing the longitudinal structure of the model's low-frequency variability. In one approach, we have used cluster analysis to group together patterns obtained on high- and low-index days. The zonal structure of the resulting clusters are particularly sensitive to the size of the sample and to the details of the distance measures used to quantify the pattern similarity of different events. The lack of robustness suggests that, although individual annular-mode events are strongly structured in longitude, there is a great deal of randomness in the longitudinal distribution of their centers, as well as in the precise details of

their structure.

In this section, we present results from a more robust, one-point correlation-map technique. This technique, which is used to define observed teleconnections, displays the auto- or lag-correlation of all points in the domain with a given spatial base point (e.g., Wallace and Gutzler, 1981). We note that this technique makes no reference to the principle-component time series of the annular mode or to the annular-mode structure itself. It thus serves as an independent means of characterizing the simulated low-frequency variability.

Figs. 9a,b display one-point auto-correlation maps, calculated at base points near 35° latitude and 65° latitude. The maps are calculated for a base point at a given latitude for all longitudes, and then rotated in longitude so that the base points coincide. Nearly identical maps are produced if only a single base point is considered. The latitudes of these two particular base points were chosen for display because they yield the largest amplitude negative center for all base points in their latitude bands. This can be seen in Fig. 10a, which displays the magnitude of the largest value of the anticorrelation as a function of base-point latitude. Note that the negative center of the first map is located close to the base point of the second map, and vice versa. Thus, the pair of maps represents a classical teleconnection.

The teleconnection in Figs. 9a,b resembles a zonally localized version of the annular-mode EOF (Fig. 4a). Consistently, small values of the amplitude of the annular mode, that occur in the tropics, near 50° latitude, and near the pole,

are matched to small values of the amplitude of the strongest anticorrelation in Fig. 10a. The one-point correlation map at the 50° latitude node base point is shown in Fig. 9c. This map consists of a single positive center and displays no teleconnection structure in the meridional direction, and only weak structure in the zonal direction. The map for a base point at the most poleward model grid-point is shown in Fig. 9d. In this case, there is a weak area of anticorrelation throughout the midlatitudes. For extratropical base-point latitudes away from the small values of the EOF, the teleconnection structure is robust, with a center of one sign between 60° and 70°, and another of opposite sign between 30° and 40° (Fig. 10b).

Given the agreement in meridional structure between the annular mode and the teleconnection, we can interpret the teleconnection as the typical local pattern present during high- or low-index annular-mode events. Of particular interest here is the zonal structure of the teleconnection. For extratropical base-point latitudes away from the node and polar regions, the pattern has a zonal extent of 60 to 90 degrees longitude. It also displays a robust northwest-southeast offset of 20° longitude between the centers (Fig. 10c). The overall pattern is reminiscent of the observed NAO (Fig. 1). As the base point is moved toward polar latitudes, the anticorrelation center becomes less localized in the zonal direction (Fig. 9d). This is expected, given the zonal homogeneity of the statistics: fluctuations with centers of action of one sign near the pole cannot favor a particular longitude for the midlatitude center of the opposite sign.

Because of the resemblance between the teleconnections and the observed NAO, we also consider the structure of the leading EOF over a limited longitudinal domain. For regions wider than 120 degrees longitude, we find the EOF has only weak zonal structure. For regions narrower than 120 degrees longitude (Fig. 11), however, the EOF takes on a structure that more closely resembles the teleconnection pattern and the observed NAO, similar to the results of Ambaum et al. (2001) and Hurrell (1995).

Since we have largely eliminated baroclinic eddies with the low-pass filter, we expect that the patterns we describe here will largely be equivalent barotropic. This is verified by examining the maps of the autocorrelation of the 500 mb (Fig. 12) and the 100 mb (Fig. 13) height fields with the surface-pressure base-point time series of Fig. 9. The general picture of the scale and location of the centers is similar at all three levels, with evidence of a modest westward phase tilt with height below 500 mb.

Finally, we use lag-correlation maps to briefly examine the temporal development of this teleconnection pattern (Fig. 14), using a base point at 35° latitude. The initial impression is that the dipole is advected consistently with the zonal-mean wind at each latitude, with easterlies advecting the poleward center and westerlies advecting the equatorward center. However, the actual phase velocity of the midlatitude center is relatively slow, approximately 5-10 degrees longitude per day, corresponding to 5-10 m/s at 35° latitude, somewhat less than the surface westerly value (Fig. 2), and much less than the mid-to-upper-tropospheric values.

Thus, the midlatitude anomalies would appear to be retrograde with respect to the tropospheric winds, which suggests the behavior of a traveling Rossby wave. For a barotropic Rossby wave,

$$U - c = \frac{\beta a^2}{n(n+1)} \tag{1}$$

where $\beta = 2\Omega \cos\theta / a^2$, a is the radius of the Earth, U is the zonal wind at the equivalent barotropic level, c the phase speed of the traveling Rossby wave, and n the total wavenumber. Fig. 14 suggests $n \approx 5$ giving $U - c \approx 20$ m/s which, for $U \approx 30$m/s, gives a value of c roughly consistent with the movement of the midlatitude center. This estimate is consistent with one determined from a longitude-time correlation plot (Fig. 15) (Robinson, 1991a).

5 Summary and Discussion

In this study, we have investigated the structure and composition of the annular mode in an atmospheric general circulation model with zonally symmetric lower boundary conditions — an 'aquaplanet.' The average fields of the model are, to within an error determined by the finite length of the model integration, zonally symmetric. In particular, the average annular-mode structure is zonally symmetric and similar to the observed northern hemisphere and southern hemisphere annular modes. However, individual annular-mode *events* are quite zonally *asymmetric.* These events are characterized by zonally localized structures with one or more strong centers. Only by averaging over many separate events

does the zonally symmetric signature of the annular mode emerge.

As the structure of the annular mode itself does not resemble that of the events which project most strongly onto it, we investigated other means of characterizing the low-frequency variability of the model. One-point correlation maps were calculated for each latitude, and these confirmed the presence of a teleconnection pattern in the meridional direction. The centers of the teleconnection are equivalent barotropic, extend into the model upper troposphere, and lie near the maxima in the annular mode, as we might expect. However, the centers are also zonally localized at each latitude, and typically do not extend all around the hemisphere, in contrast with the structure of the model annular mode. The centers are typically offset in longitude by approximately 20°. The low-frequency variability of the model is thus characterized by meridional dipoles in the sea-level pressure, with centers near 35° and 65° latitude, and a zonal scale of $60^\circ - 90^\circ$. Because these events are distributed uniformly in longitude in the aqua-planet model, they are represented in an EOF analysis as a single, zonally uniform pattern. Examination of individual high- and low-index annular-mode events reveals a similar picture: most events can be broadly characterized by a single major center at midlatitudes, and a somewhat broader anomaly of opposite sign near the polar region. Embedded within this general pattern are numerous, weaker centers of smaller scale. Due to the presence of these noisy features, individual events will of course exhibit significant departures from the structure of the teleconnection pattern, as well as from that of the annular mode. However, by capturing the

characteristic zonal scale, as well the typical zonal offset in the positive and negative anomalies, the teleconnection is more representative of the typical structure of the low-frequency variability than is the annular mode. Consistent with this picture of individual events, the leading EOFs calculated over limited regions of the model domain have structures similar to the teleconnection maps.

The discrepancy between the structure of the annular mode and the underlying events implies that the annular mode in our model is a statistical feature, rather than a particular zonally symmetric mode of variability. The annular mode arises out of the unrotated EOF analysis, which is well known to be unreliable in representing structures in the underlying data (Richman, 1986), particularly when the domain is larger than the dominant scales of variability. The other tests we performed failed to produce a robust zonally symmetric structure. Now, one might expect an aquaplanet model to be one of the most promising candidates in which to find a large scale, zonally homogeneous feature. Specifically, one might expect zonally symmetric modes to be *more* important in this model than they are in the real atmosphere. The fact that in such a model the annular mode does not directly represent the low-frequency variability suggests that zonally symmetric variability is not a direct cause of the observed low-frequency variability.

Of course, it is possible that the annular mode in the real atmosphere behaves in a quite different way than in our model. However, the one point correlations maps calculated near the maxima of the annular mode do resemble the observed NAO in structure. Since the model's zonally asymmetric structures do resemble

those of the atmosphere, it seems unlikely that the dynamics of the zonally symmetric behavior of the model would be completely different. Thus, we suggest that the annular mode is not a zonally symmetric mode of variability *per se,* but that it is the composite result of many zonally inhomogeneous events each with a similar meridional structure. It is not clear whether this is true in the real atmosphere. Nevertheless, the results presented here suggest that it is necessary to better understand the relationship between the observed annular mode and the (potentially zonally asymmetric) underlying data, on timescales characteristic of the events themselves, before any conclusions may be unequivocally drawn about role of zonally symmetric modes of low-frequency variability in the atmosphere.

Acknowledgements

We are grateful for comments from Isaac Held and Gabriel Lau, as well as two anonymous reviewers. GKV also acknowledges funding from the NSF.

References

Ambaum, M. H. P., B. J. Hoskins, and D. B. Stephenson, 2001. Arctic Oscillation or North Atlantic Oscillation? *J. Climate*, **14**, 3495–3507.

Barnston, A. G., and R. E. Livezey, 1987. Classification, seasonality, and persis-

tence of low-frequency atmospheric circulation patterns. *Mon. Wea. Rev.*, **115**, 1083–1126.

Cash, B. A., and S. Lee, 2001. Observed nonmodal growth of the Pacific-North American teleconnection pattern. *J. Climate*, **14**, 1017–1028.

Feldstein, S. B., 2000. Is interannual zonal mean flow variability simply climate noise? *J. Climate*, **13**, 2356–2362.

Feldstein, S. B., and S. Lee, 1996. Mechanisms of zonal index variability in an aquaplanet GCM. *J. Atmos. Sci.*, **53**, 3541–3556.

Gong, D., and S. Wang, 1999. Definition of Antarctic Oscillation index. *Geophys. Res. Lett.*, **26**, 459–462.

Hendon, H. H., and D. L. Hartmann, 1985. Variability in a nonlinear model of the atmosphere with zonally symmetric forcing. *J. Atmos. Sci.*, **42**, 2783–2797.

Hurrell, J. W., 1995. Decadal trends in the North Atlantic Oscillation: Regional temperatures and precipitation. *Science*, **269**, 676–679.

Hurrell, J. W., 1996. Influence of variations in extratropical wintertime teleconnections on Northern Hemisphere temperature. *Geophys. Res. Lett.*, **23**, 665–668.

Hurrell, J. W., and H. van Loon, 1997. Decadal variations in climate associated with the North Atlantic Oscillation. *Climatic Change*, **36**, 301–326.

Limpasuvan, V., and D. L. Hartmann, 2000. Wave-maintained annular modes of climate variability. *J. Climate*, **13**, 4414–4429.

Manabe, S., D. G. Hahn, and J. L. Holloway, 1979. Climate simulation with GFDL spectral models of the atmosphere. GARP Publ. Ser. No. 22. WMO, Geneva.

Richman, M. B., 1986. Rotation of principal components. *J. Climatol.*, **6**, 293–333.

Robinson, W. A., 1991a. The dynamics of low-frequency variability in a simple model of the global atmosphere. *J. Atmos. Sci.*, **48**, 429–441.

Robinson, W. A., 1991b. The dynamics of the zonal index in a simple model of the atmosphere. *Tellus*, **43A**, 295–305.

Simmons, A. J., and D. M. Burridge, 1981. An energy and angular-momentum conserving vertical finite-difference scheme and hybrid vertical coordinates. *Mon. Wea. Rev.*, **109**, 758–766.

Thompson, D. W. J., and J. M. Wallace, 1998. The Arctic Oscillation signature in the wintertime geopotential height and temperature fields. *Geophys. Res. Lett.*, **25**, 1297–1300.

Thompson, D. W. J., and J. M. Wallace, 2000. Annular modes in the extratropical circulation. Part I: Month-to-month variability. *J. Climate*, **13**, 1000–1016.

van Loon, H., and J. C. Rogers, 1978. The seesaw in winter temperatures between

Greenland and northern Europe. part I: General description. *Mon. Wea. Rev.*, **106**, 296–310.

Wallace, J. M., 2000. North Atlantic Oscillation / Annular Mode: Two paradigms - one phenomena. *Quart. J. Roy. Meteor. Soc.*, **126**, 791–805.

Wallace, J. M., and D. S. Gutzler, 1981. Teleconnections in the geopotential height field during the Northern Hemisphere winter. *Mon. Wea. Rev.*, **109**, 784–812.

Yu, J.-Y., and D. L. Hartmann, 1993. Zonal flow vacillation and eddy forcing in a simple GCM of the atmosphere. *J. Atmos. Sci.*, **50**, 3244–3259.

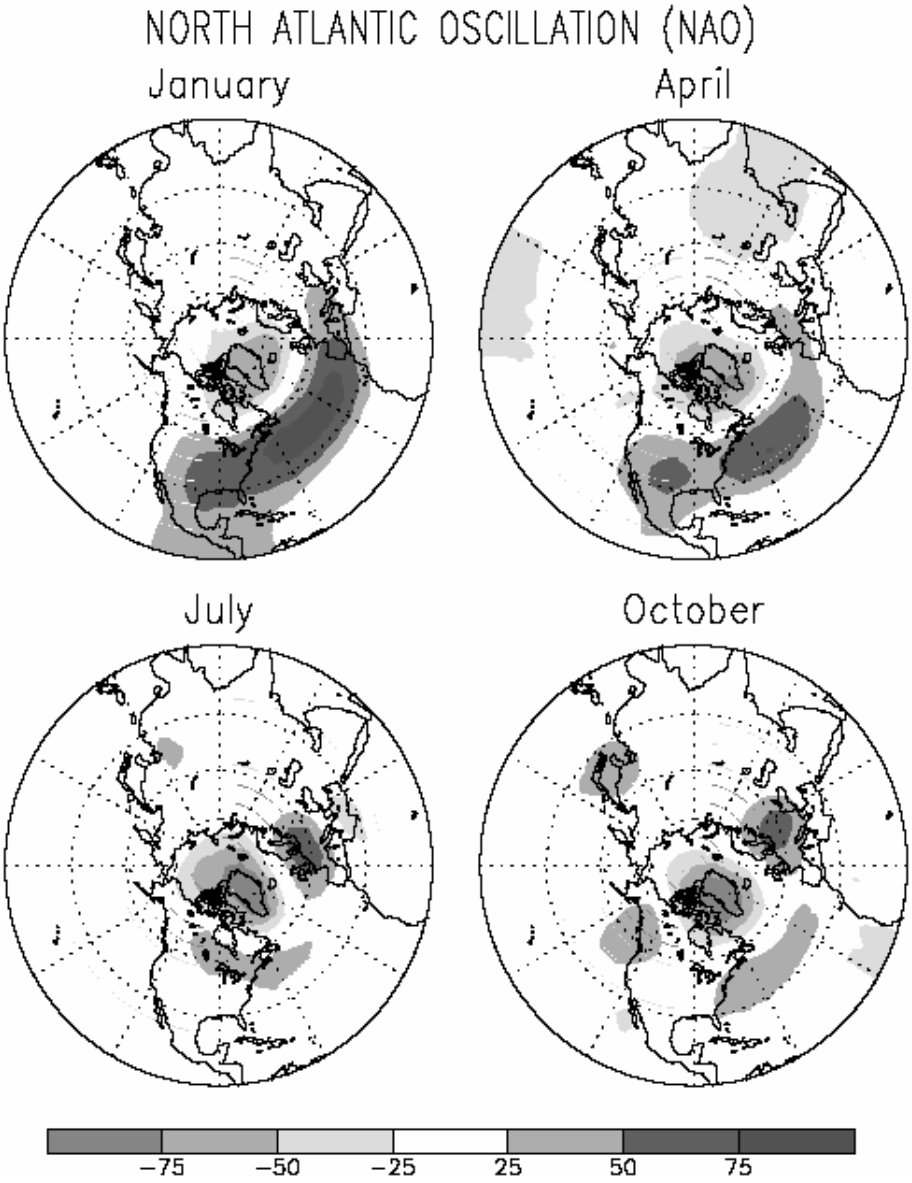

Figure 1: North Atlantic Oscillation, following Barnston and Livezey (1987). Panels show NAO pattern as determined from monthly mean 700 mb height anomalies by rotated principle component analysis for the listed months from 1964-1994. Figures are displayed as monthly mean height anomalies, and are taken from Climate Prediction Center web site (http://www.cpc.ncep.noaa.gov).

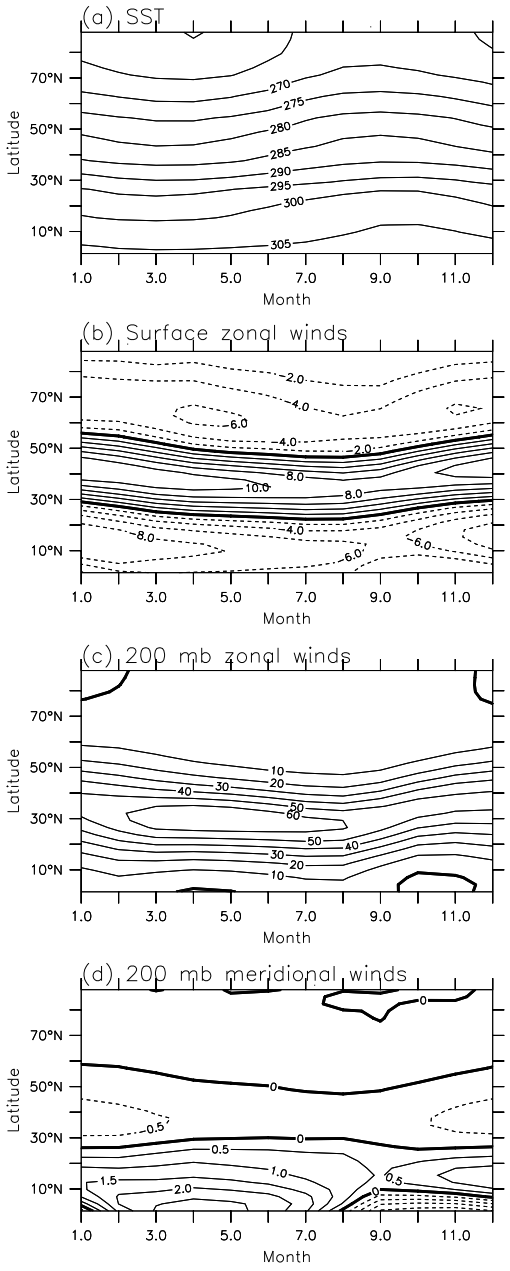

Figure 2: Model climatology for each month. Fields are, (a) zonal mean sea surface temperatures, (b) zonal mean zonal winds at surface, (c) zonal mean zonal winds at 200 mb, and (d) zonal mean meridional winds at 200 mb. Horizontal axis represents time in months, with month 1 corresponding to January.

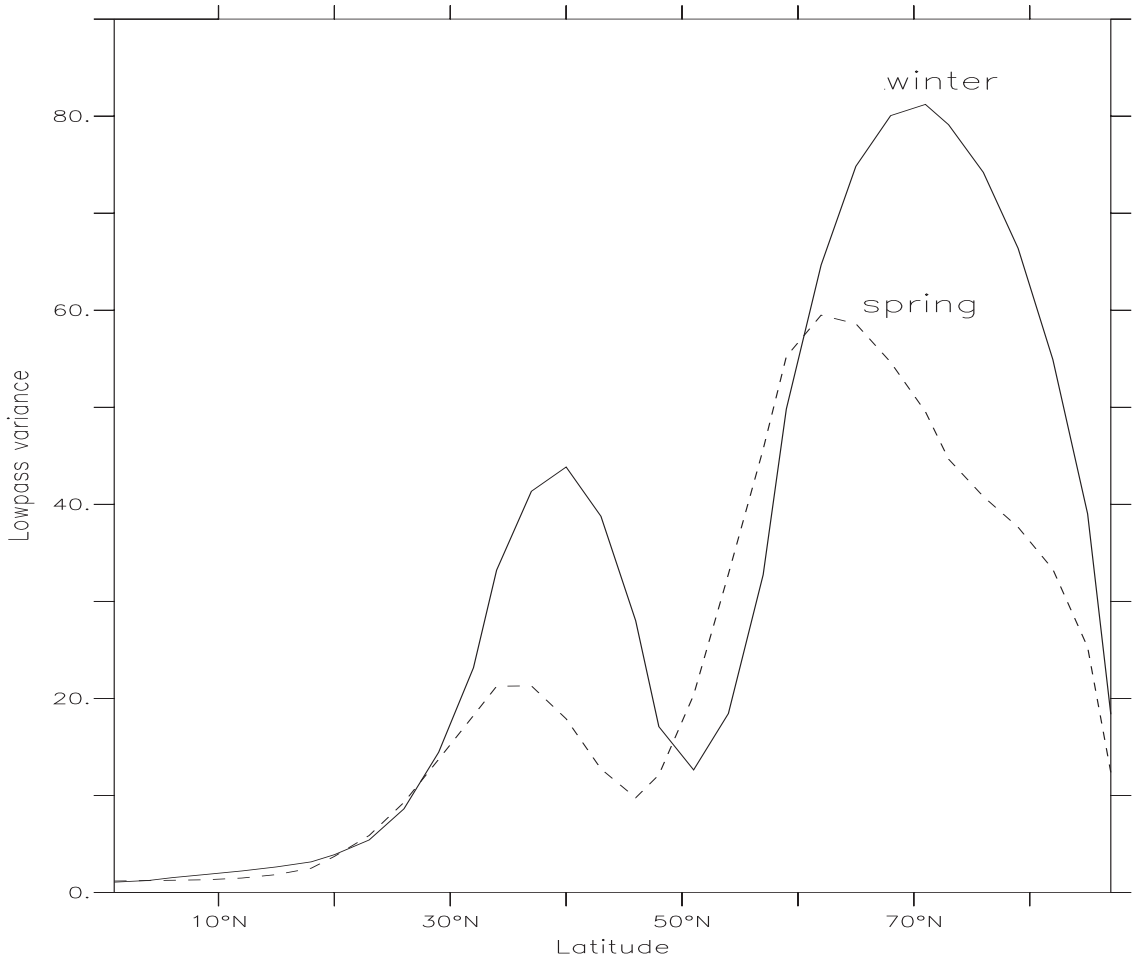

Figure 3: Seasonal low-frequency variability. Solid line is zonal mean 'winter' mean variance of the de-seasonalized 10-day low-pass filtered surface pressure, and dashed line is mean 'spring' variance. Winter and spring are defined as given in the text. Units are mb^2.

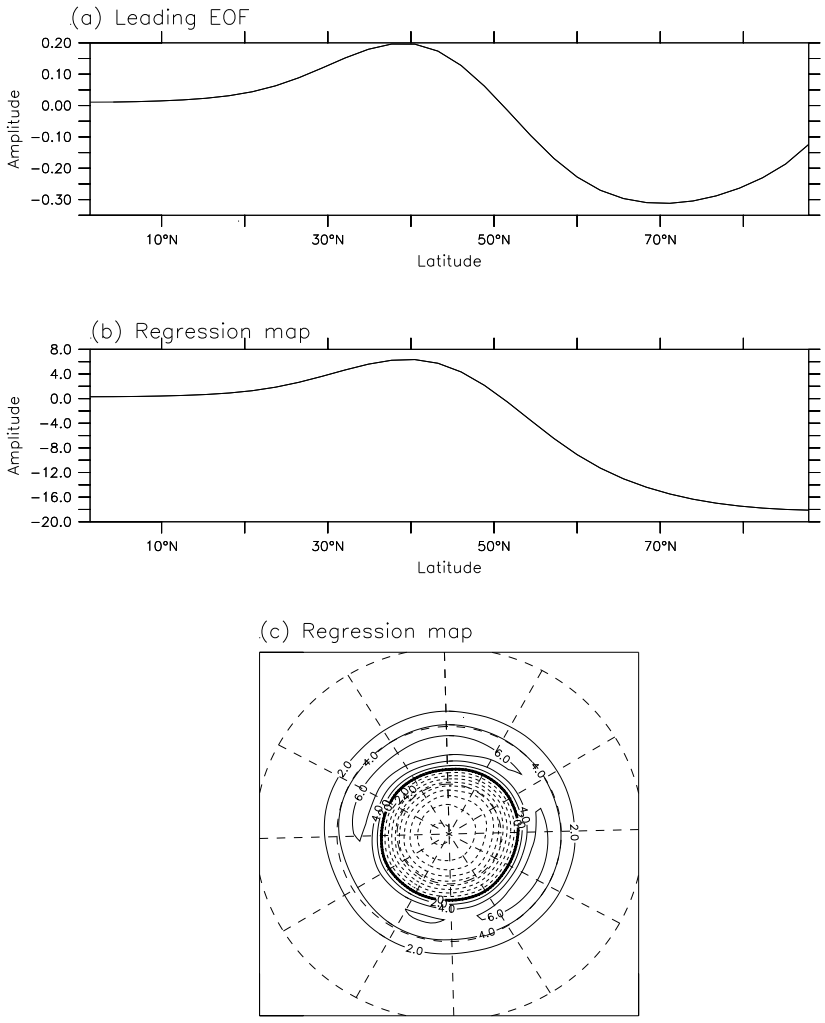

Figure 4: Leading EOF of winter season surface pressure. (a) Normalized, nondimensional EOF of the zonal mean surface pressure. (b) Regression map of zonal mean surface pressure against the principal component of the leading EOF. Amplitude is the response to one standard deviation in the principal component. Units are mb. (c) As in (b), except for the zonally varying pressure. Solid lines are positive, dashed lines are negative, and a heavy contour denotes the zero line. Contour interval is 2 mb.

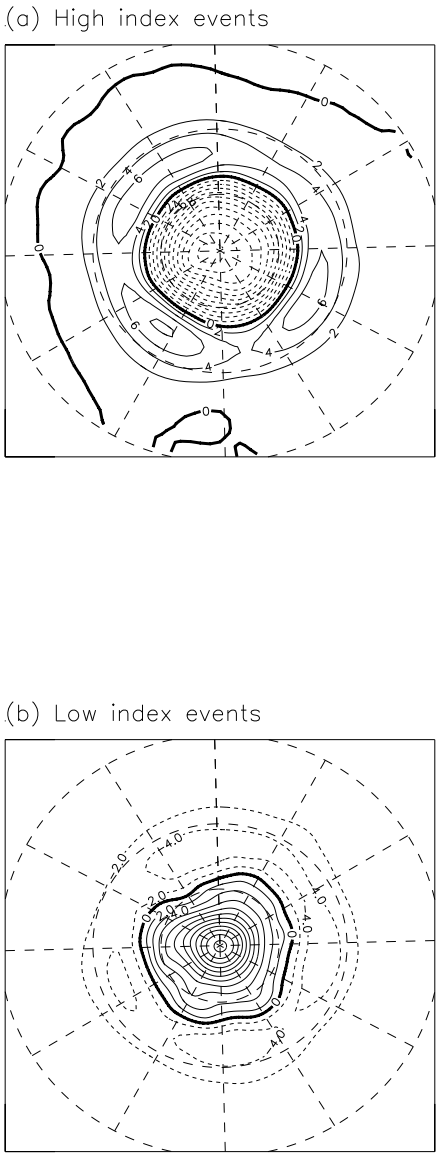

Figure 5: Composite surface pressure for (a) high-index events (71 events) and (b) low-index events (64 events). Solid contours are positive, dashed contours are negative, and a heavy contour denotes the zero line. Contour interval is 2 mb. The deviations from zonal symmetry are due to the finite length of the integration.

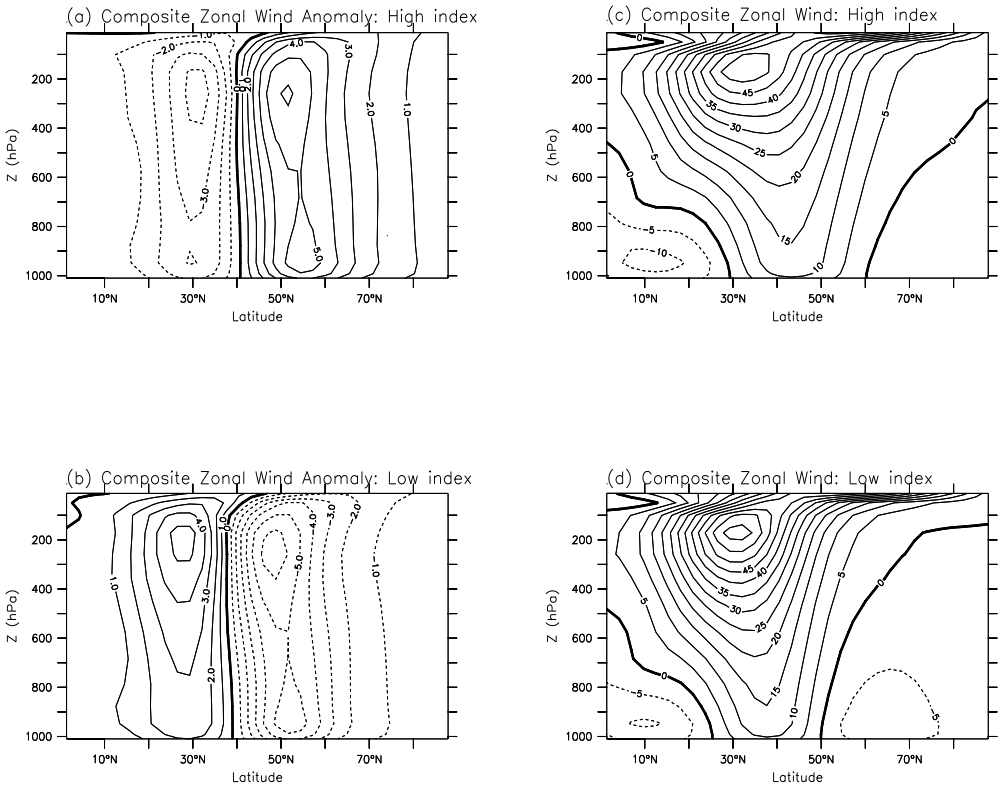

Figure 6: Composite anomalous zonal winds for (a) high-index events, (b) low-index events, (c) total composite zonal winds for high-index events, (d) total composite zonal winds for low-index events.

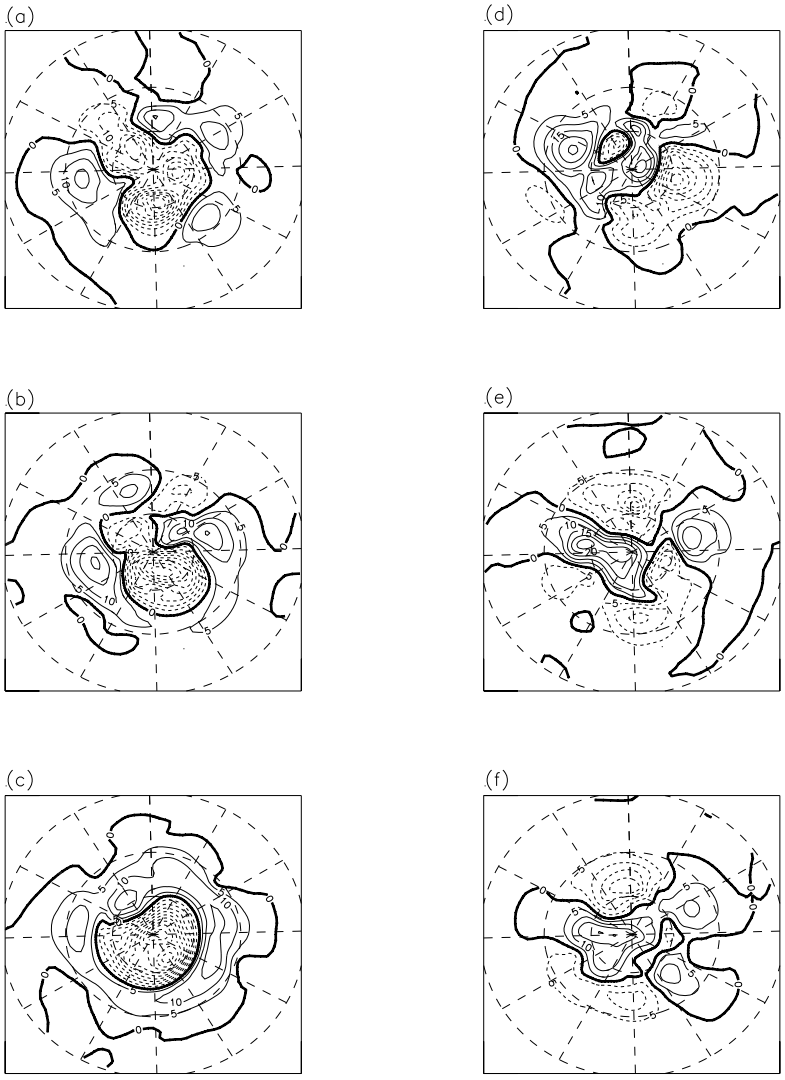

Figure 7: High- and low-index annular-mode events. Panels (a), (b), and (c) are high-index events, (d), (e), and (f) are low-index events. Events displayed are 3 day averages about the day that the projection coefficient attains its maximum value during the event. Solid contours are positive, dashed contours are negative, and a heavy contour denotes the zero line. Contour interval is 5 mb.

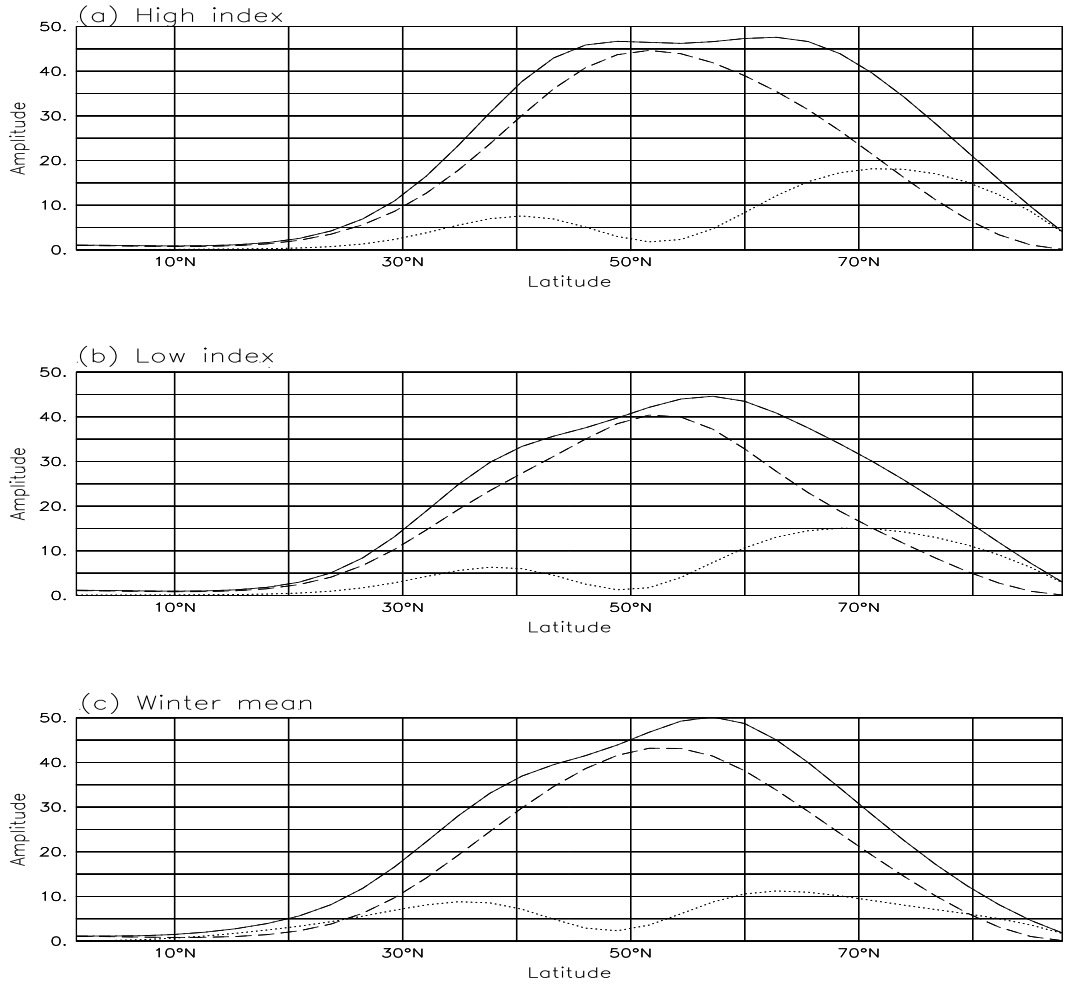

Figure 8: Composite spectral amplitude for (a) high-index (71 events), (b) low-index (64 events), and (c) full winter. Solid lines denote the total amplitude, dashed lines the eddy component, and dotted lines the zonal mean component, as defined in the text. Units are mb^2.

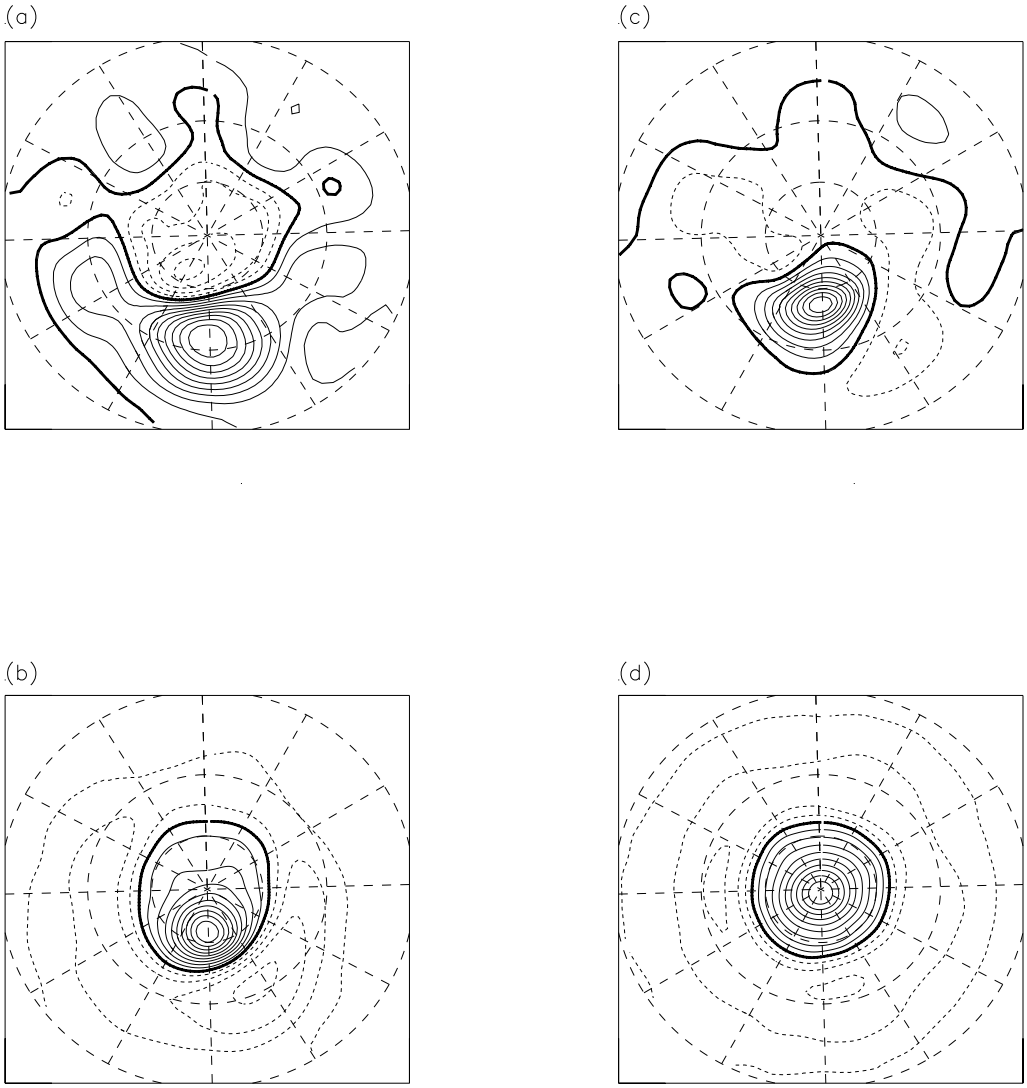

Figure 9: One-point correlation maps for surface pressure. (a) Base point at 35°, (b) base point at 65°, and (c) base point at 50°, and (d) base point at pole. Solid contours are positive, dashed contours are negative, and a heavy contour denotes the zero line. Contour interval is 0.1. Correlation maps are averages taken over all longitudes, for a given latitude, where base points have been rotated to coincide.

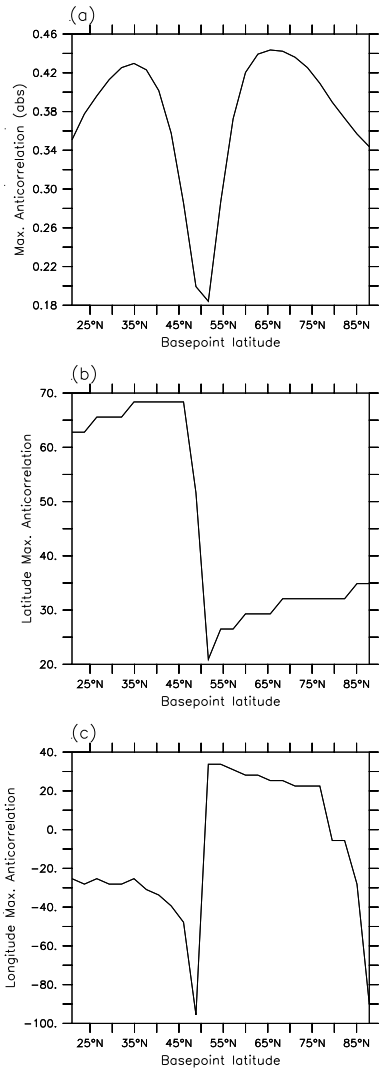

Figure 10: Teleconnections in low-frequency flow. (a) Magnitude of the maximum anticorrelation as a function of base point latitude. (b) Latitude of the maximum anticorrelation as a function of base point latitude. (c) Longitudinal offset of the maximum anticorrelation from the longitude of the base point as a function of base point latitude.

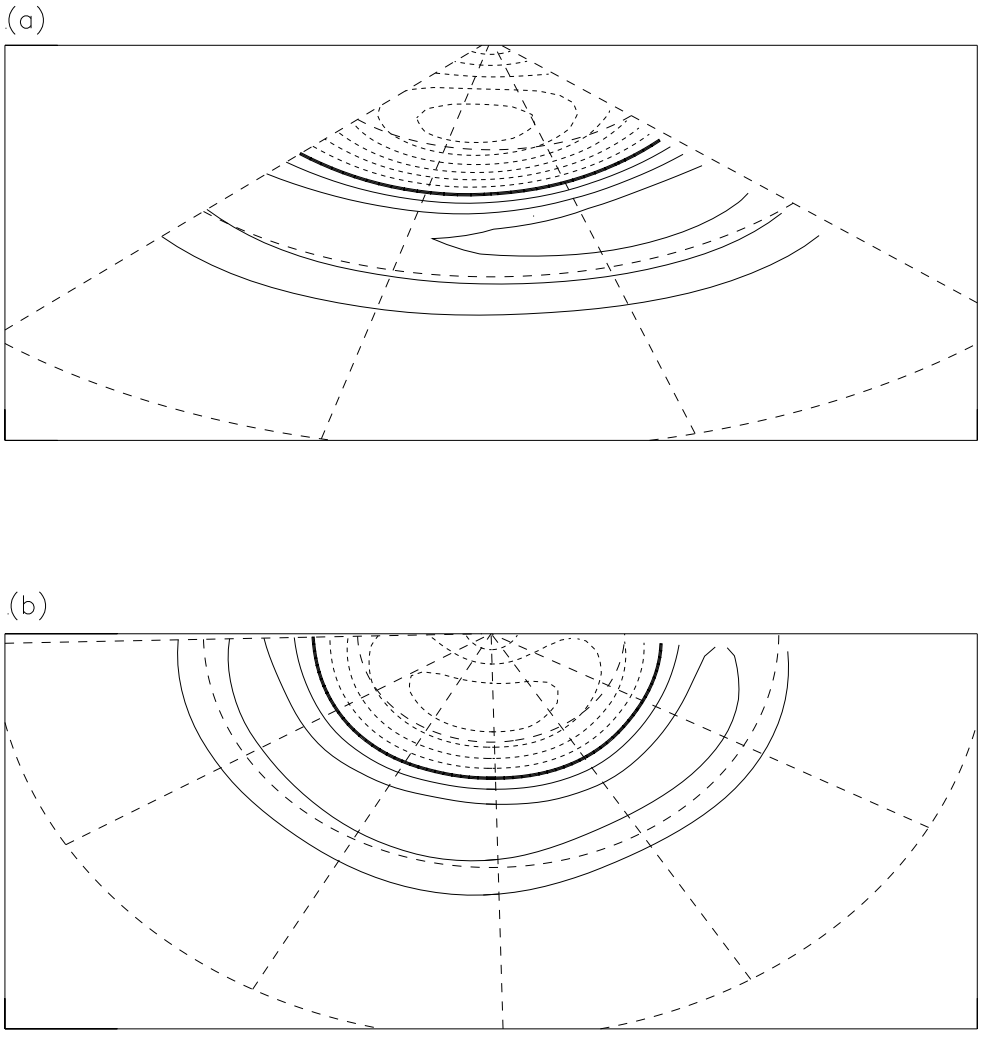

Figure 11: Leading EOF for surface pressure for limited domains. EOF is calculatedfor (a) a domain 90° longitude by 90° latitude, and (b) 180° longitude by 90° latitude. The data set is the same used in Fig. 4.

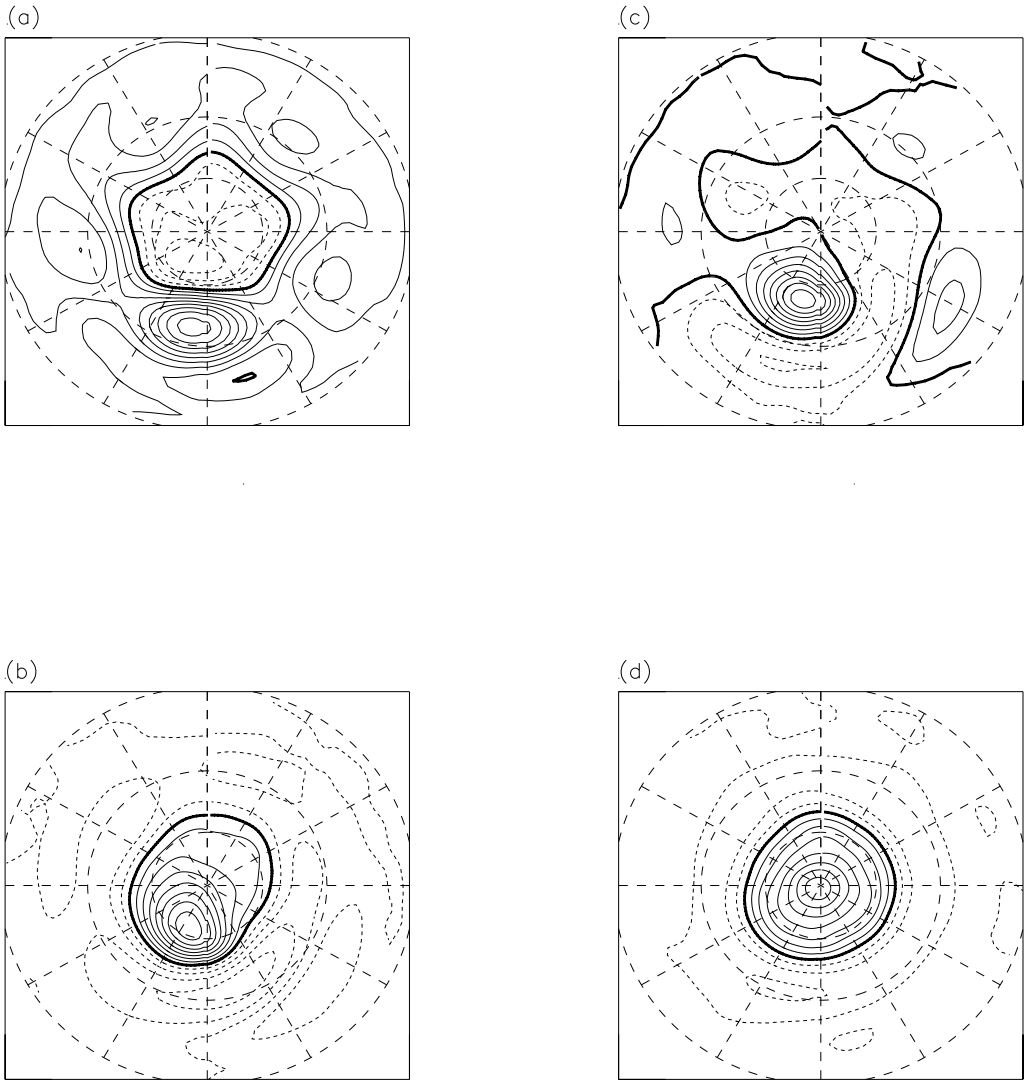

Figure 12: As in Figure 9, except correlations are taken between the surface pressure at the base point and the 500 mb height field.

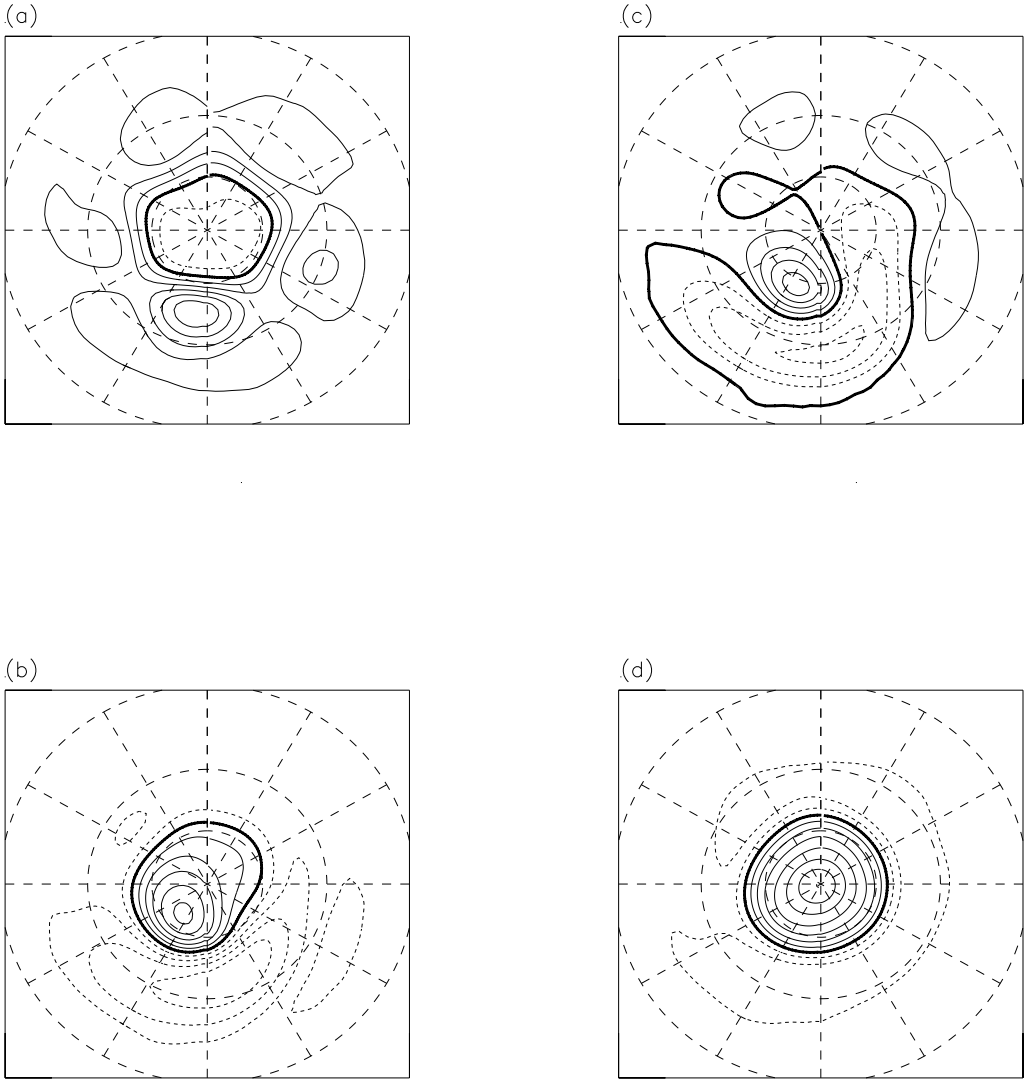

Figure 13: As in Figure 12, except for the 100 mb height field.

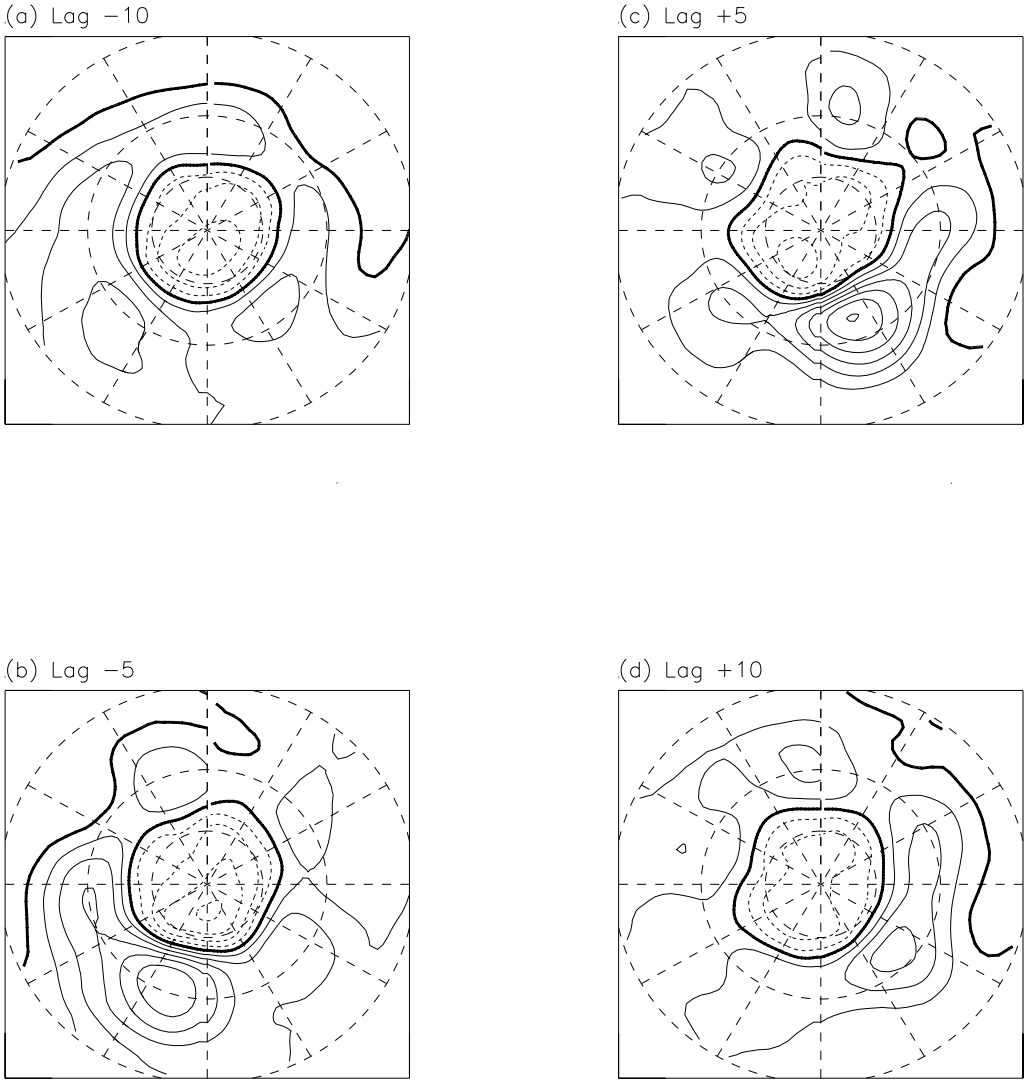

Figure 14: One-point lag-correlation maps of surface pressure for base point at 35° latitude and (a) lag -10 days, (b) lag -5 days, (c) lag +5 days, and (d) lag +10 days. Solid contours are positive, dashed contours are negative, and a heavy contour denotes the zero line. Contour interval is 0.1.

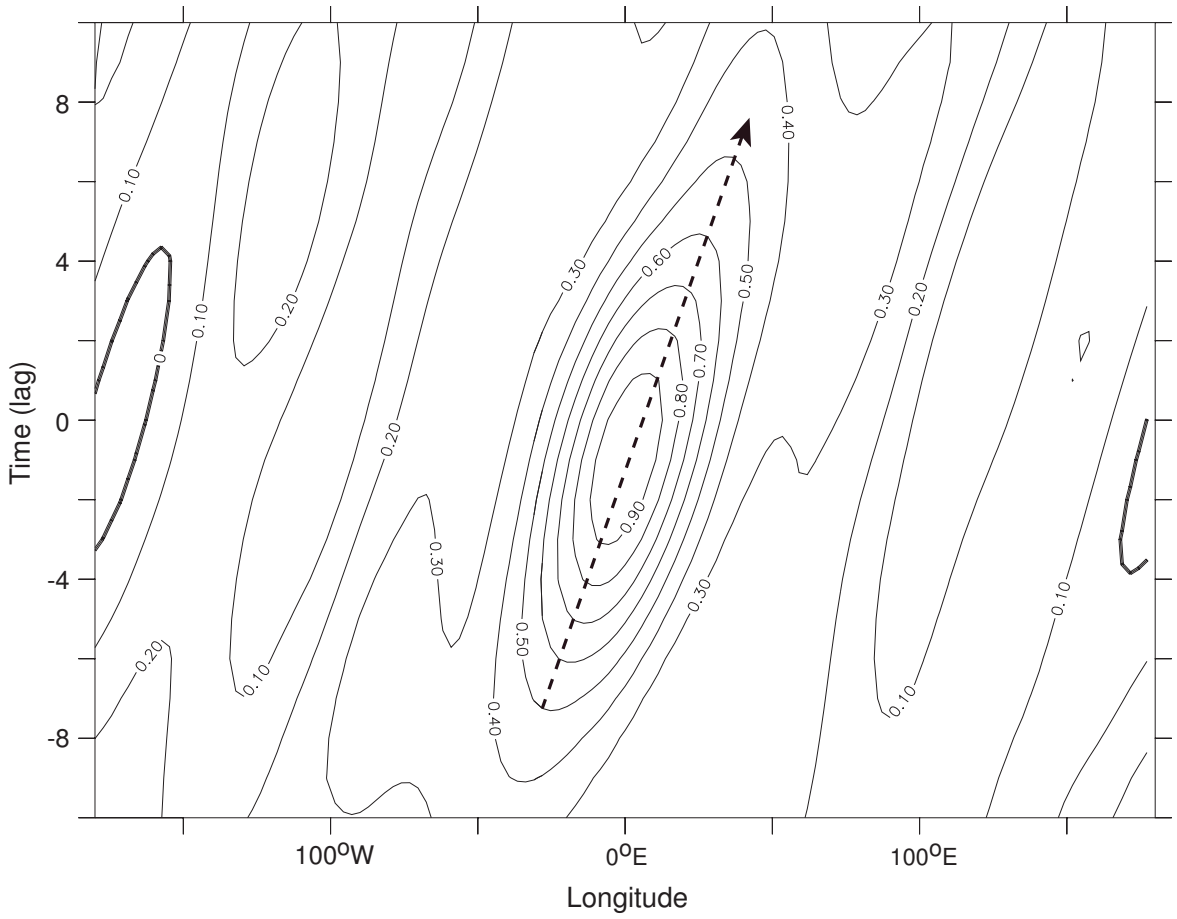

Figure 15: One-point longitude-time correlation map of surface pressure for base point at 35°. Solid contours are positive, dashed contours are negative, and a heavy contour denotes the zero line. Dashed arrow indicates a phase speed of approximately 5° longitude per day. Contour interval is 0.1.